Research Paper

Earthquake Spectra
42:e70029
DOI: 10.1002/esp4.70029

Incorporating Ground Motion Directionality into Probabilistic Seismic Hazard Analysis

Alan Poulos,[1] M.EERI, and Eduardo Miranda,[1] M.EERI

Abstract

Probabilistic seismic hazard analysis (PSHA) is typically used to estimate a ground motion intensity measure representing a central tendency within the horizontal plane, such as the median intensity across all horizontal orientations. However, in many cases, ground motion intensity is needed in specific horizontal orientations, particularly along the principal response axes of structures. Depending on the earthquake source, path effects, and site conditions, a site may exhibit significant levels of ground motion directionality, that is, a variation in ground motion intensity within the horizontal plane. If such variations are systematic across the earthquakes that affect the site, they can lead to significant differences in ground motion intensity between horizontal orientations. This paper introduces directional PSHA, an extension of conventional PSHA that quantifies seismic hazard for a specified horizontal orientation. The method primarily involves adapting the outputs of existing ground motion models to be orientation-specific. The approach is applied to strike-slip earthquakes, which tend to produce above-average ground motion intensity in the transverse orientation. Two simple case studies are used to illustrate the method: a line-segment fault and the San Francisco Bay Area, limited to the San Andreas and Hayward Faults. Results show strong orientation dependence in seismic hazard at sites located very close to a strike-slip fault. Similar levels of orientation dependence are found at sites located farther from the fault relative to its length. The proposed method offers a more detailed description of the seismic hazard at a site and can improve seismic risk assessment methods for both new and existing structures.

Keywords

PSHA, seismic hazard, ground motion directionality, ground motion intensity, response spectra

[1] Department of Civil and Environmental Engineering, Stanford University, Stanford, CA, USA

Corresponding author:
Alan Poulos, Department of Civil and Environmental Engineering, Stanford University, 473 Via Ortega, Stanford, CA 94305, USA.
Email: apoulos@alumni.stanford.edu

Introduction

A probabilistic description of ground motion intensity is essential for many earthquake engineering applications, including the development of seismic hazard maps (e.g., Petersen et al. 2024), assessment of seismic risk (McGuire 2004), and performance-based structural design. This description is typically obtained through probabilistic seismic hazard analysis (PSHA; Esteva 1967, 1968; Cornell 1968), which computes the exceedance rates of a ground motion intensity measure, such as horizontal pseudo-spectral acceleration. Although most of these intensity measures exhibit significant variation within the horizontal plane, ground motion models (GMMs) used in PSHA usually consider a single scalar value, such as the geometric mean of the two as-recorded horizontal components or the median intensity across all horizontal orientations (RotD50, following the notation introduced by Boore 2010). However, there are many cases in which ground motion intensities at specific horizontal orientations (azimuths) are of interest. For example, due to their geometry and the arrangement of their lateral-force-resisting elements, most structures (e.g., buildings and bridges) have two perpendicular horizontal principal axes. Thus, depending on the orientation of the structure, ground motion intensities along these axes of interest may exceed or fall below the RotD50 intensity.

The variation of ground motion intensity within the horizontal plane, usually known as ground motion directionality, has been attributed to several phenomena that can polarize seismic waves, such as topographic irregularities (e.g., Spudich et al. 1996), near-surface geological structures (e.g., Bonamassa and Vidale 1991), basin edge effects (e.g., Ktenidou et al. 2016), and rupture directivity (e.g., Somerville et al. 1997). However, predicting the specific orientations in which higher or lower-than-average intensities tend to occur has, in general, remained elusive. While a few studies have characterized the variation of pseudo-spectral acceleration probabilistically as a function of the angular distance from the orientation of maximum pseudo-spectral acceleration (Hong and Goda 2007; Poulos and Miranda 2022a), this maximum orientation is still required to estimate values at specific horizontal orientations.

By evaluating ground motions in the NGA-West2 database (Ancheta et al. 2014), Poulos and Miranda (2023a) recently found that strike-slip earthquakes tend to produce the maximum pseudo-spectral acceleration within the horizontal plane at an orientation close to the transverse orientation, that is, an orientation perpendicular to the line segment between the site of interest and the epicenter. This observation was then verified in recent strike-slip earthquakes in Taiwan (Poulos and Miranda 2024), California (Girmay et al. 2024a), and Türkiye (Girmay et al. 2024b). Consequently, Poulos and Miranda (2023b) proposed a probabilistic model for strike-slip earthquakes to modify the median pseudo-spectral acceleration (RotD50) and obtain pseudo-spectral accelerations in any specific horizontal orientation, with this ground-motion intensity decreasing as the orientation of interest moves away from the transverse orientation. This model can therefore be used together with any ground motion model (GMM) developed for RotD50 (e.g., Boore et al. 2014) to conduct PSHA for pseudo-spectral acceleration at specific horizontal orientations.

This paper proposes an extension of PSHA, called directional PSHA, that computes mean annual exceedance rates of a ground motion intensity measure at a specific horizontal orientation. The method is developed to estimate 5%-damped pseudo-spectral acceleration at specific orientations by using the model proposed by Poulos and Miranda (2023b). Two simple examples are used to illustrate the proposed directional PSHA method and to identify cases where its results vary significantly with changes in horizontal orientation, and hence where its adoption would lead to better estimates of ground motion intensity.

Orientation-dependent ground motion intensity

In earthquake engineering, ground motion intensity is usually characterized by response spectral ordinates, which correspond to peak responses of a linear elastic oscillator with a specific period of vibration and a specific damping ratio (usually 5%). For a given ground motion record and period, this peak response can depend significantly on the horizontal orientation of interest. For example, Figure 1 shows the bidirectional relative displacement trace (hodogram) of a 5%-damped linear elastic oscillator with a vibration period of 5 s subjected to both horizontal components of ground motion from the 1999 M_W 7.1 Hector Mine, California, earthquake recorded at the LAX Fire Station. Spectral displacements at any specific orientation (azimuth), depicted in Figure 1b as the distance from the origin (i.e., the resting position of the oscillator) to the black line, can be computed as the maximum absolute displacement within the corresponding orientation (see, for example, Poulos and Miranda 2022b). The maximum intensity across all possible orientations is commonly referred to as RotD100 (Boore 2010) and, in this case, is 116% larger than the minimum intensity across all possible orientations (RotD00). Several studies have shown that this difference tends to increase as the period of the oscillator becomes longer (e.g., Hong and Goda 2007; Poulos and Miranda 2022a).

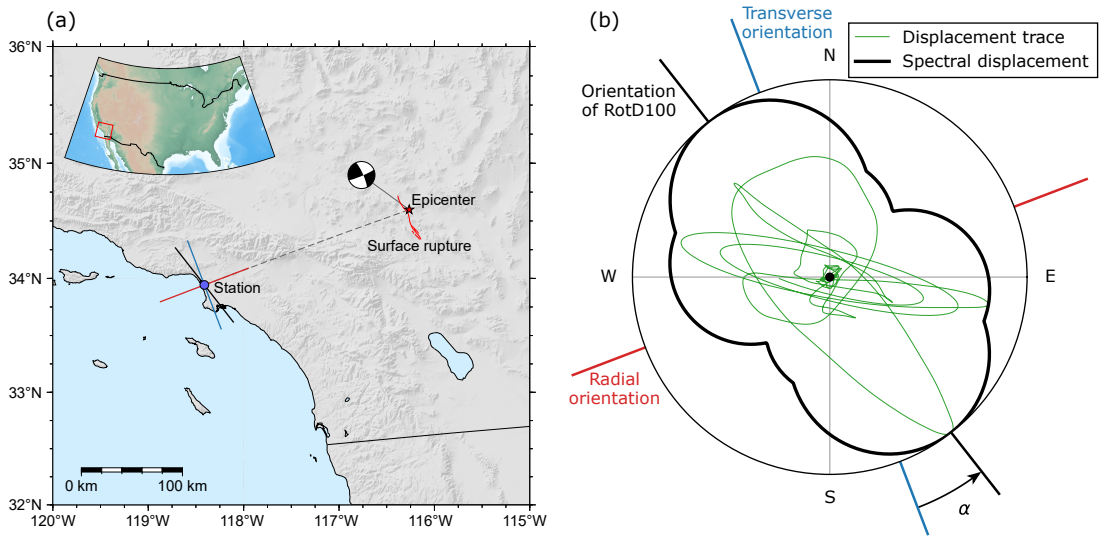

Figure 1. Ground motion from the 1999 M_W 7.1 Hector Mine earthquake recorded at the LAX Fire Station: (a) location of the earthquake and site, and (b) relative displacement hodogram and spectral displacements of a 5-s oscillator. The transverse, radial, and RotD100 orientations are depicted using blue, orange, and black lines, respectively. The surface rupture is from (Treiman et al. 2002). The upper-left inset of panel (a) shows the location of the main map.

By studying ground motions from earthquakes with strike-slip faulting in the NGA-West2 database (Ancheta et al. 2014), Poulos and Miranda (2023a) found that the orientation of RotD100 tends to be close to the transverse orientation, that is, an orientation perpendicular to the line segment that joins

the recording station to the epicenter. For the example record, the orientation of RotD100 is relatively close to the transverse orientation, with the angular distance between these orientations, $|\alpha|$, being only 17° (Figure 1). The orientation of RotD100 tends to be even closer to the transverse orientation as the period of the oscillator becomes longer (Poulos and Miranda 2023a). As an example, Figure 2 shows the orientations of RotD100 for oscillators with periods of 5 and 10 s at 119 stations that recorded the 1999 M_W 7.1 Hector Mine earthquake. The orientations of RotD100 tend to be closer to the transverse orientation in the 10-s case than in the 5-s case, with the mean $|\alpha|$ values being 11.0° and 27.6°, respectively. However, even for the 5-s case, the mean $|\alpha|$ is still relatively low compared to a scenario where RotD100 orientations are random and sampled from a uniform distribution, in which the mean $|\alpha|$ is 45°.

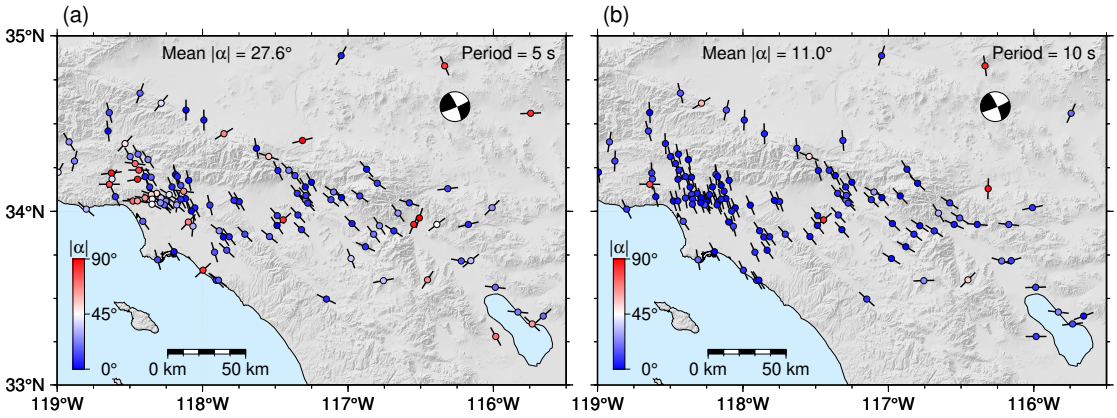

Figure 2. Orientations of RotD100 for (a) 5-s and (b) 10-s oscillators subjected to horizontal ground motions of the 1999 M_W 7.1 Hector Mine earthquake. The circles represent recording stations and are colored to depict the angular distance between the orientation of RotD100 and the transverse orientation at each site. The corresponding mean angular distances are presented at the top of each panel.

Given the observations of Poulos and Miranda (2023a), Poulos and Miranda (2023b) studied the variation of pseudo-spectral accelerations as a function of their angular distance to the transverse orientation, denoted here by θ. In order to compare the variations among records with different intensities, the pseudo-spectral accelerations are normalized by the median intensity across all horizontal orientations (RotD50), leading to the following γ ratio:

$$\gamma(\theta) = \frac{Sa(\theta)}{Sa_{\text{RotD50}}} \tag{1}$$

where $Sa(\theta)$ is a pseudo-spectral acceleration at an orientation of interest θ away from the transverse orientation, and Sa_{RotD50} is the RotD50 pseudo-spectral acceleration. Using ground motions from the NGA-West2 database (Ancheta et al. 2014) recorded during strike-slip earthquakes, Poulos and Miranda (2023b) fitted regression models to several statistics of the γ ratio, of which the geometric mean and logarithmic standard deviation are shown in Figure 3. The models depend only on the period of the oscillator and on θ. The geometric means of Figure 3a show that, on average, pseudo-spectral accelerations decrease when moving away from the transverse orientation, that is, as θ increases.

Furthermore, the variation of pseudo-spectral acceleration with θ becomes more significant as the period increases. If the epicenter is known, then the transverse orientation can be determined for any site, and these models can be combined with any GMM developed for the RotD50 intensity to estimate pseudo-spectral accelerations at any specific horizontal orientation.

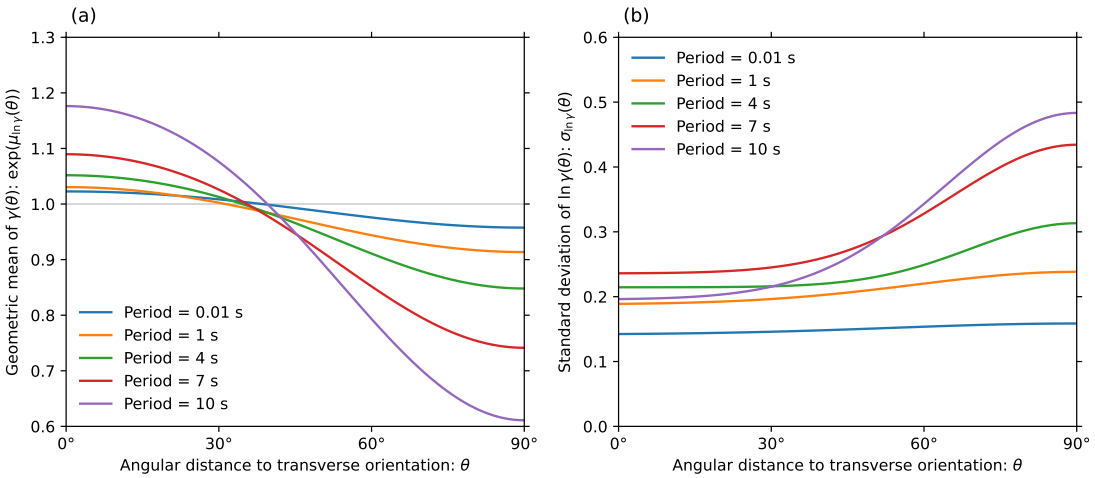

Figure 3. Statistics of the $\gamma(\theta) = Sa(\theta)/Sa_{\text{RotD50}}$ ratio from Poulos and Miranda (2023b) for different periods and angular distances to the transverse orientation: (a) geometric mean and (b) logarithmic standard deviation.

Incorporating orientation-dependent horizontal intensities in PSHA

The objective of PSHA is to compute the seismic hazard curve at a given site of interest, that is, the mean annual rate of exceedance of different levels of a ground motion intensity. The ground motion intensity is usually characterized by a measure of central tendency of horizontal intensities, such as the geometric mean of the two as-recorded horizontal components or, more recently, by RotD50. PSHA usually estimates the seismic hazard at a given site by using a finite set $\mathcal{R}$ of earthquake rupture scenarios. The seismic hazard curve at the site, λ_{IM}, is then computed as the weighted average of the probabilities of exceedance of each scenario, with the weights being the mean annual rates of each of the scenarios:

$$\lambda_{IM}(x) = \sum_{r \in \mathcal{R}} \lambda_r P(IM_r > x) \tag{2}$$

where λ_r is the mean annual rate of occurrence of rupture scenario r and $P(IM_r > x)$ is the probability of exceeding a certain level of ground motion intensity $IM = x$ for rupture scenario r, which is computed by assuming that the ground motion intensity measure is lognormally distributed:

$$P(IM_r > x) = 1 - \Phi\left(\frac{\ln(x) - \mu_{\ln IM_r}}{\sigma_{\ln IM_r}}\right) \tag{3}$$

where $\Phi(\cdot)$ is the cumulative distribution function of a standard normal random variable; and $\mu_{\ln IM_r}$ and $\sigma_{\ln IM_r}$ are, respectively, the mean and standard deviation of the logarithm of the ground motion intensity for rupture scenario r, which are given by a GMM. These GMM parameters depend on the rupture itself (e.g., earthquake magnitude, style of faulting, and hypocenter depth), some characteristic of the path (e.g., source-to-site distance), and the site conditions, which are usually considered using the time-averaged shear-wave velocity to 30 m depth (V_{S30}).

The seismic hazard curve at a given site can then be computed with the following steps:

1. Characterize the seismic hazard of the site by a set of earthquake rupture scenarios, each with an associated mean annual rate of occurrence.
2. Evaluate the mean and standard deviation of the ground motion intensity for each rupture scenario using a GMM.
3. Computed the conditional probabilities of exceedance of the ground motion intensity for each rupture scenario using Equation (3).
4. Compute the hazard curve by combining all rupture scenarios using Equation (2).

The high-level procedure to conduct PSHA explained previously can be modified to compute a seismic hazard curve but now for a ground motion intensity at a specific horizontal orientation ψ, denoted here as $\lambda_{IM|\Psi}$:

$$\lambda_{IM|\Psi}(x,\psi) = \sum_{r\in\mathcal{R}} \lambda_r P(IM_r(\psi) > x) \tag{4}$$

where $IM_r(\psi)$ is the ground motion intensity at orientation ψ for rupture scenario r. The difference is that now the mean and standard deviation of the logarithm of the ground motion intensity are computed for a specific horizontal orientation ψ:

$$P(IM_r(\psi) > x) = 1 - \Phi\left(\frac{\ln(x) - \mu_{\ln IM_r}(\psi)}{\sigma_{\ln IM_r}(\psi)}\right) \tag{5}$$

The way in which the mean, $\mu_{\ln IM_r}(\psi)$, and standard deviation, $\sigma_{\ln IM_r}(\psi)$, at the specific horizontal orientation ψ are computed could vary depending on the cause of directionality that is being considered and the model that is being used. One option is to modify a GMM developed for a scalar intensity, such as RotD50 or the geometric mean of the two as-recorded components. This study uses the model recently developed by Poulos and Miranda (2023b) to modify the pseudo-spectral accelerations computed with a GMM developed for RotD50. Specifically, the mean logarithm from a RotD50 GMM, $\mu_{\ln IM_r}$, is modified by adding the mean logarithm of γ, $\mu_{\ln\gamma}$, which is the same as the logarithm of the geometric mean γ shown in Figure 3a:

$$\mu_{\ln IM_r}(\psi) = \mu_{\ln IM_r} + \mu_{\ln\gamma}(\theta_r(\psi)) \tag{6}$$

where $\theta_r(\psi)$ is the angular distance from the orientation of interest ψ to the transverse orientation of rupture scenario r. Additionally, the logarithmic standard deviation is modified using the logarithmic standard deviation of γ, $\sigma_{\ln\gamma}$, and the correlation coefficient between the logarithm of the RotD50 intensity and the logarithm of γ, $\rho_{\ln IM_r,\ln\gamma}$:

$$\sigma^2_{\ln IM_r}(\psi) = \sigma^2_{\ln IM_r} + \sigma^2_{\ln\gamma}(\theta_r(\psi)) + 2\sigma_{\ln IM_r}\sigma_{\ln\gamma}(\theta_r(\psi))\rho_{\ln IM_r,\ln\gamma}(\theta_r(\psi)) \tag{7}$$

where $\sigma_{\ln IM_r}$ is the logarithmic standard deviation from a from a RotD50 GMM. (Poulos and Miranda 2023b) provide values for $\mu_{\ln\gamma}$, $\sigma_{\ln\gamma}$, and $\rho_{\ln IM_r,\ln\gamma}$. Note that the modification of the GMM is site and rupture scenario-specific because it depends on angle θ, which in turn depends on the position of the site of interest relative to the epicenter and whose computation is shown schematically in Figure 4. Thus, the modification has to be integrated within the PSHA computations, that is, incorporated in Equations (6) and (7) for each rupture scenario prior to considering all scenarios in Equation (4). Perhaps other sources of ground directionality, such as local geological structures and topography, could in some cases be modeled as scenario independent, and directional PSHA could be considered as a post-processing step of a conventional RotD50 PSHA, therefore decoupling both analyses.

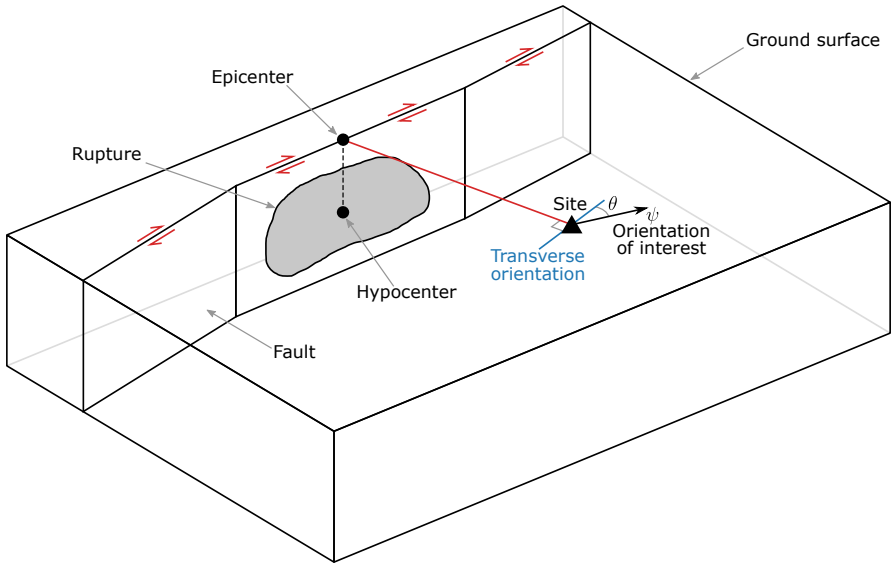

Figure 4. Diagram showing the computation of angle θ (i.e., the angle between the transverse orientation and the orientation of interest ψ) for a given site, earthquake rupture scenario on a strike-slip fault, and horizontal orientation of interest required for directional PSHA.

To summarize, the seismic hazard curve at a given site and specific orientation of interest ψ can be computed with the following steps:

1. Characterize the seismic hazard of the site by a set of earthquake rupture scenarios, each with an associated mean annual rate of occurrence.
2. Evaluate the mean and standard deviation of the ground motion intensity for each rupture scenario using a GMM.
3. Compute the transverse orientation at the site of interest for each rupture scenario.
4. Compute the angle θ between the transverse orientation and the orientation of interest ψ.
5. Modify the mean and standard deviation from the GMM to make them orientation-specific using Equations (6) and (7).

6. Compute the conditional probabilities of exceedance of the ground motion intensity for each rupture scenario using Equation (5).
7. Compute the hazard curve by combining all rupture scenarios using Equation (4).

Simple illustrative example calculations

Two simple examples are presented to illustrate the use of the proposed directional PSHA method: a basic line-segment fault and a simplified seismic hazard case for the San Francisco Bay Area that considers only the San Andreas and Hayward Faults. These examples also help identify cases where the results of directional PSHA differ from those of conventional, orientation-independent PSHA and thus warrant its use.

Line-segment fault

The first case consists of a line-segment seismic source representing a vertically dipping strike-slip fault that generates earthquakes with moment magnitudes ranging from 4 to 7. The length of the fault is initially set to 50 km, although lower and higher values are also tested. The frequency of earthquakes is given by a Gutenberg-Richter magnitude frequency distribution with parameters $a = 4$ and $b = 1$ (Ishimoto and Iida 1939; Gutenberg and Richter 1944). Ruptures are assumed to be vertical planes with lengths given by the magnitude-dependent empirical relation developed by Wells and Coppersmith (1994). The GMM used is that developed by Boore et al. (2014) to estimate RotD50 pseudo-spectral accelerations, and a V_{S30} of 500 m/s is considered for all sites used in the analysis.

The first site considered is located collinear with the fault, at a distance of 5 km from the edge of the fault, as shown in the top right corner of Figure 5a. The proposed directional PSHA method is first used to compute hazard curves of pseudo-spectral acceleration at 5 s for two specific orientations: north-south (N–S) and east-west (E–W), as shown in Figure 5a. For the site considered in this first example, the transverse orientation always coincides with the N–S orientation, regardless of the epicenter location. Consequently, the pseudo-spectral acceleration in the N–S orientation has mean annual rates of exceedance higher than those corresponding to the RotD50 pseudo-spectral acceleration. Conversely, the pseudo-spectral acceleration in the E–W orientation has mean annual rates of exceedance lower than those of the RotD50 pseudo-spectral acceleration because, for the considered site, the E–W orientation always coincides with the radial orientation. Figure 5a also highlights the intensities corresponding to return periods of 475 and 2475 years, which correspond to intensities with probabilities of exceedance of 10% and 2% in 50 years, respectively, values that are commonly used in earthquake-resistant design. For the 475-year return period, the intensities in the N–S and E–W orientations are, respectively, 8.5% higher and 16.2% lower than the RotD50 intensity. Relatively similar values are obtained for the 2475-year return period, with the intensity in the N–S and E–W orientations being 11.8% higher and 15.9% lower, respectively.

The same analysis is then repeated to compute seismic hazard curves at all possible horizontal orientations to obtain the intensities that correspond to return periods of 475 and 2475 years. Figure 5b shows these intensities in a polar representation, that is, the intensity at any specific orientation is given by the distance from the corresponding line (475 or 2475 years) at that orientation to the origin. As expected, the orientations that maximize and minimize the resulting intensities are the N–S and E–W orientations, respectively. Orientations near the N–S orientation have intensities higher than the corresponding RotD50

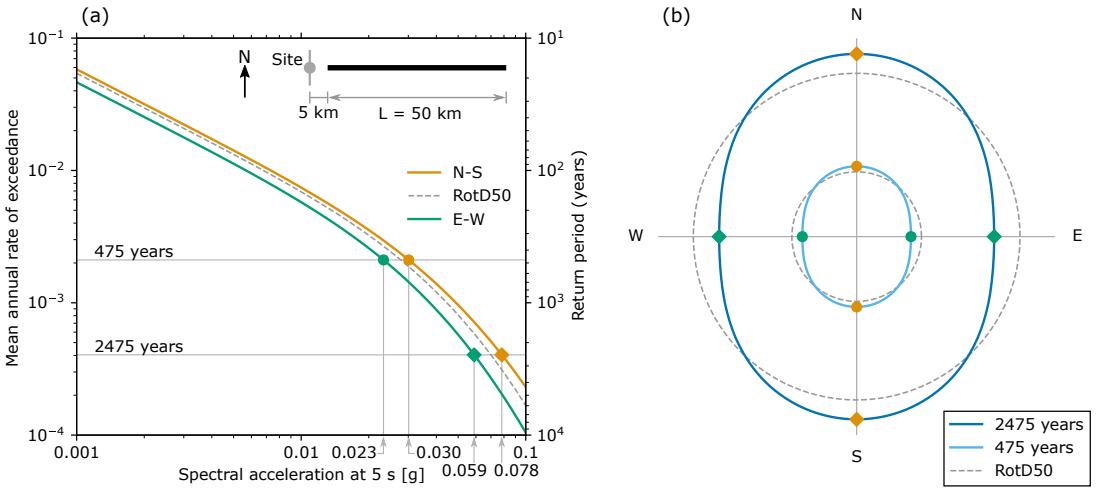

Figure 5. Seismic hazard results for pseudo-spectral acceleration at 5 s at the selected site: (a) hazard curves at the north-south (N–S) and east-west (E–W) orientations compared to the median across all horizontal orientations (RotD50), and (b) directional uniform hazard pseudo-spectral acceleration at return periods of 475 and 2475 years compared to the corresponding RotD50 seismic hazard (gray dashed circles). The top right of panel (a) shows a map view of the selected site relative to the fault.

intensity, with orientations where this occurs representing 44% and 48% of all possible orientations for the 475- and 2475-year return period cases, respectively.

Repeating the previous analysis for a range of periods, instead of just 5 s, and computing the 475- and 2475-year return period intensities leads to the uniform hazard spectra at the N–S and E–W orientations shown in Figure 6a. Regardless of the return period, the uniform hazard spectra associated with the N–S orientation (which coincides with the transverse orientation in this example) are larger than those associated with RotD50, which would be the result of a conventional PSHA. Conversely, the response spectra associated with the E–W orientation (which coincides with the radial orientation in this example) are lower than those associated with RotD50. Furthermore, the difference between the RotD50 spectra and either the N–S or E–W spectra increases as the period becomes longer, which is consistent with the geometric mean ratios from the Poulos and Miranda (2023b) model (see Figure 3a).

To quantify the effect of orientation on seismic hazard results, this work uses the maximum divided by the minimum pseudo-spectral acceleration from all orientations, which is denoted by ω:

$$\omega = \frac{\max\limits_{\psi \in [0°, 180°)} Sa(\psi)}{\min\limits_{\psi \in [0°, 180°)} Sa(\psi)}$$

where $Sa(\psi)$ is the pseudo-spectral acceleration at an orientation ψ for a specific return period (either 475 or 2475 years). For the example site and line-segment fault shown in Figure 5a, the maximum and minimum pseudo-spectral accelerations occur in the N–S and E–W orientations, respectively, and the

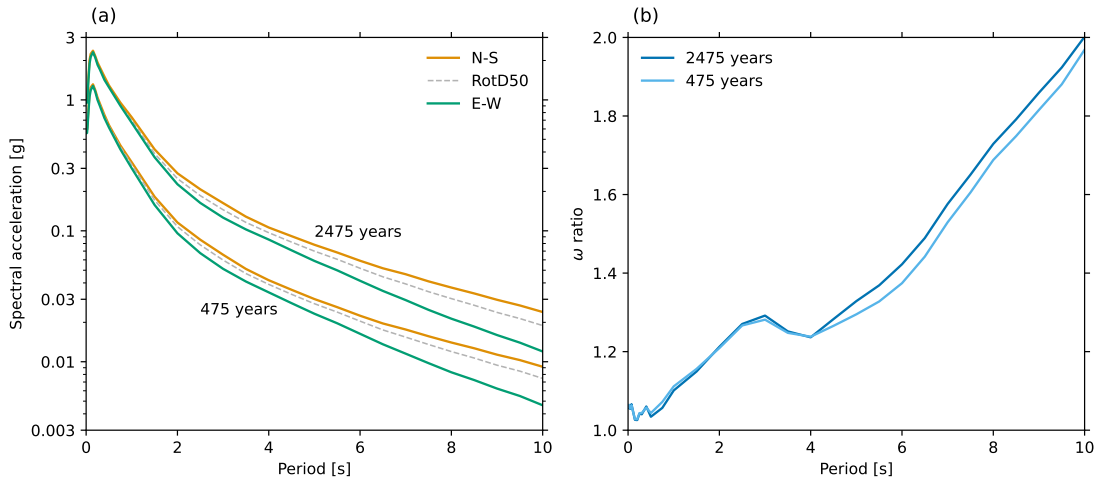

Figure 6. Uniform seismic hazard results at the selected site for return periods of 475 and 2475 years: (a) uniform hazard spectra at the north-south (N–S) and east-west (E–W) orientations compared to the median across all horizontal orientations (RotD50), and (b) maximum to minimum pseudo-spectral acceleration ratios (ω) as a function of period.

ω ratio increases as the period becomes longer (Figure 6b). Hence, the seismic hazard from directional PSHA becomes more orientation-dependent and more distinct from that of conventional, orientation-independent PSHA.

The level of orientation dependence of directional PSHA changes depending on the location of the site relative to the fault. To illustrate this effect, two additional sites shown in Figure 7 are analyzed: one located 5 km from the edge of the fault (Site B) and another located 10 km from the midpoint of the fault (Site C). The two new sites show variations in seismic hazard with orientation that are very different from the original site (Site A), with Site C showing essentially the same seismic hazard across all orientations and Site B showing its maximum hazard at 26° clockwise from the N–S orientation. It is important to note that the orientation of maximum intensity at each site does not necessarily correspond to the transverse orientation of specific rupture scenarios. Rather, it is the outcome of the integration of all rupture scenarios, where rupture length, position, and epicenter are randomized.

To simplify the comparison of the level of orientation dependence of directional PSHA across all sites surrounding the fault, a single value is compared for each site, corresponding to the ω ratio for the pseudo-spectral acceleration at 5 s and a return period of 2475 years. These ratios are shown in Figure 8 for faults of lengths 1, 50, 100, and 150 km, with the fault length studied previously shown in Figure 8b. The figure also presents the orientations of the maximum pseudo-spectral acceleration at each site. For the case of the 1 km fault (Figure 8a), all epicenters are essentially located at the same point, resulting in all earthquakes having the same transverse orientation and a uniform ω ratio of approximately 1.34 across sites. As the fault lengthens, two regions begin to appear on either side of the fault where the transverse orientation varies significantly between different earthquake epicenters, resulting in weaker orientation dependence of directional PSHA and ω ratios closer to 1. Sites far from the fault relative to the length of

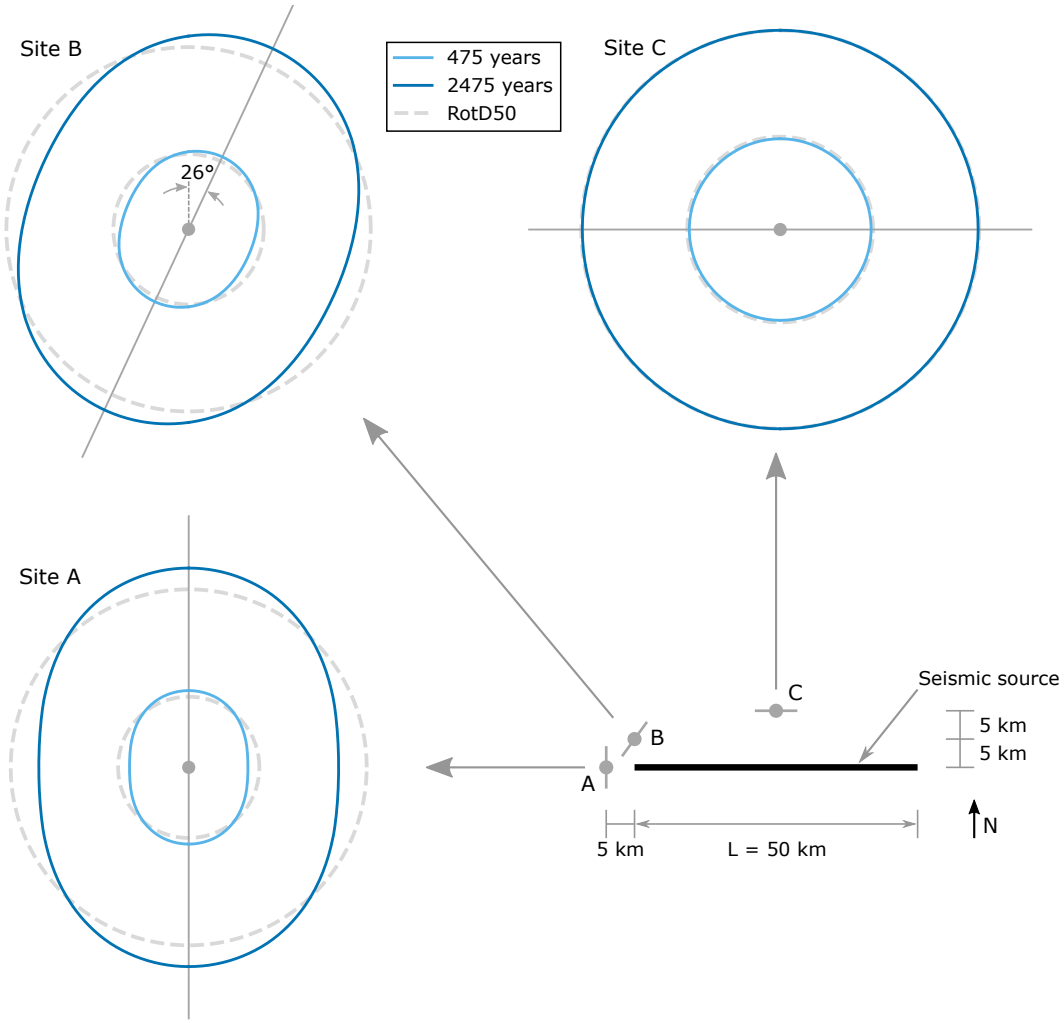

Figure 7. Directional uniform seismic hazard results at three selected sites for oscillators with periods of vibration of 5 s and return periods of 475 and 2475 years. The gray lines at each site represent the orientations of maximum hazard, and the dashed circles represent the RotD50 hazard. The bottom-right illustration is a map view of the three selected sites relative to the fault.

the fault continue to have high ω ratios because the transverse orientation does not vary significantly as the earthquake epicenter changes. Interestingly, sites located directly on the fault or relatively collinear to it show high ω ratios, regardless of the fault length. This behavior occurs because, for these sites, the transverse orientation remains perpendicular or nearly perpendicular to the fault trace.

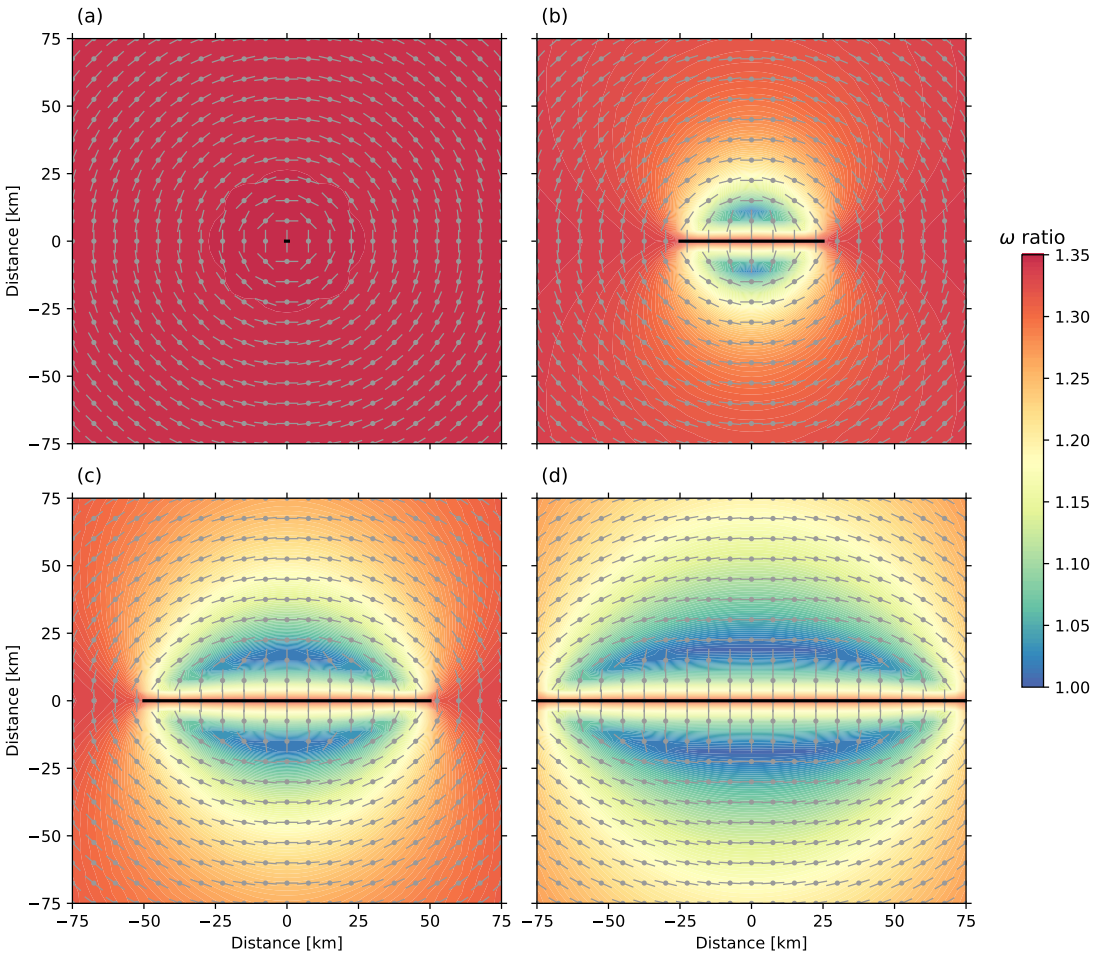

Figure 8. Spatial distribution of the maximum to minimum pseudo-spectral acceleration ratio (ω) at 5 s, for a 2475-year return period, and considering line-segment faults of lengths (a) 1 km, (b) 50 km, (c) 100 km, and (d) 150 km. Different sites are depicted by gray circles, and the gray lines correspond to the orientations of maximum pseudo-spectral acceleration at each site. The black line of each panel represents the fault.

San Francisco Bay Area

The previous example considered a single line-segment fault; however, most sites are affected by several seismic sources, which would generally reduce the level of orientation dependence of directional PSHA as the contribution of other sources increases. This effect is exemplified here by considering a simplified PSHA of the San Francisco Bay Area, which considers only the two most important faults that affect this region of California: the San Andreas and Hayward Faults. For the sake of simplicity and to better

illustrate the effects of directionality, other seismic sources were not considered. The geometry and earthquake rates of each of the two faults were obtained from the Uniform California Earthquake Rupture Forecast Version 3 (UCERF3) model (Field et al. 2014). Sites were considered to have constant V_{S30} values of 500 m/s, and the same GMM as before was used (i.e., Boore et al. 2014).

Similar to the results for the simple line-segment fault case, sites near the San Andreas and Hayward Faults have large ω ratios and, therefore, a greater degree of orientation dependence in seismic hazard (Figure 9). For pseudo-spectral acceleration at 5 s and a return period of 2475 years, the ω ratio exceeds 1.25 within a band centered on the San Andreas Fault with a width ranging from 10 to 14 km, and the band where the ω ratio is greater than 1.2 has a width that fluctuates between 15 and 25 km (Figure 9b). In contrast, sites near the Hayward Fault have lower ω ratios and narrower bands. For instance, the band where the ω ratio is greater than 1.2, centered on the Hayward Fault, is only about 7 to 9 km wide. This difference arises because the rate of earthquakes on the Hayward Fault is significantly lower than that on the San Andreas Fault. As a result, the seismic hazard at sites near the Hayward Fault is significantly affected by earthquakes on the San Andreas Fault, reducing orientation dependence, whereas the seismic hazard near the San Andreas Fault is almost unaffected by earthquakes on the Hayward Fault. Additional seismic hazard analyses that consider each fault individually (Figures S1 and S2 of the supplemental material for this article) further emphasize the stronger influence of the San Andreas Fault on sites near the Hayward Fault, compared to the influence of the Hayward Fault on sites near the San Andreas Fault. The ω ratios for pseudo-spectral acceleration at shorter periods are lower than those at 5 s, consistent with the modeled directionality effect (Figure 3a). For example, the mean ω ratios at 2 and 5 s across the region are 1.10 and 1.15, respectively; however, the relative spatial distribution among sites remains largely unchanged (Figure 9a).

Conclusions

This study proposes an extension of probabilistic seismic hazard analysis (PSHA) that can be used to obtain orientation-dependent hazard estimates. The proposed method computes mean annual rates of exceedance of a ground motion intensity measure (i.e., a hazard curve) at any specific azimuth of interest. Of the several phenomena that can cause the seismic hazard at a site to be orientation-dependent, this work focuses on the predominance of the transverse orientation in ground motions from earthquakes with strike-slip faulting. The method modifies the ground motion model used in PSHA, which considers the median (i.e., RotD50) pseudo-spectral acceleration from all horizontal orientations, to estimate pseudo-spectral accelerations at a specific orientation of interest. This modification increases pseudo-spectral accelerations near the transverse orientation and decreases them near the radial orientation.

The method was first applied to a simple line-segment fault generating strike-slip earthquakes. Results show that sites collinear with the fault (such as those directly above it) and sites located far from the fault relative to its length have seismic hazard results with strong orientation dependence, which increases with period. For example, the pseudo-spectral acceleration at 5 s with a return period of 2475 years can be 34% higher in the orientation where it reaches its maximum intensity relative to the orientation where the minimum intensity occurs, and this percentage can be as high as 100% for a period of 10 s. The method was then applied to the semi-realistic setting of the San Francisco Bay Area, affected by the two most important faults in this region of California: the San Andreas and Hayward Faults. Sites close to these faults were found to be significantly affected by ground motion directionality. However,

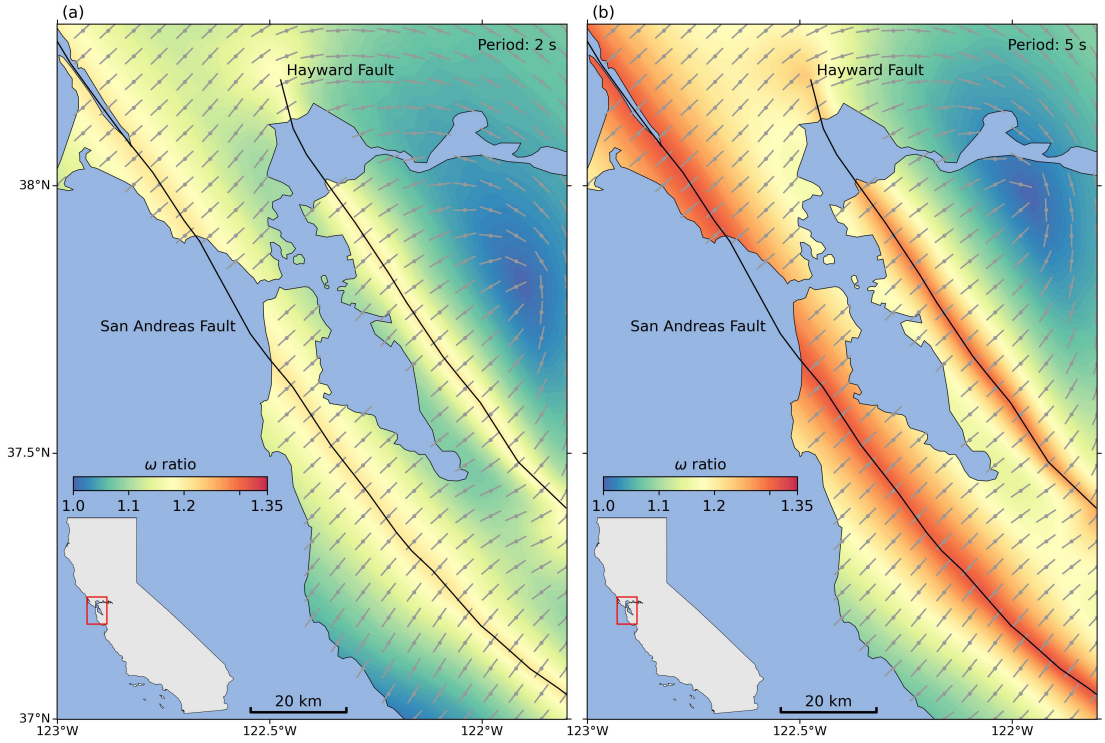

Figure 9. Spatial distribution within the San Francisco Bay Area of the maximum to minimum pseudo-spectral acceleration ratio (ω) at (a) 2 s and (b) 5 s for a 2475-year return period, considering the San Andreas and Hayward Faults. Different sites are depicted by gray circles, and the gray lines correspond to the orientations of maximum pseudo-spectral acceleration at each site. The lower-left inset shows the location of the map within California.

the orientation dependence of the seismic hazard at some sites can be smaller than that computed using a single fault. This is particularly true for sites on top of the Hayward Fault because they are significantly affected by earthquakes on the San Andreas Fault. Future studies could test how these results change in a more realistic setting, considering additional faults with varying styles of faulting. Moreover, the method could be extended to consider other phenomena that cause ground motion directionality, such as rupture directivity and the effect of subsurface geological structures (e.g., sedimentary basins).

Having seismic hazard estimates at specific horizontal orientations can be an important input for the seismic design of structures, especially those that have structural properties that are significantly orientation-dependent. Moreover, these estimates can improve seismic risk analyses of structures, since current methods do not consider the horizontal orientation of the structures. In other words, if a structure were to be rotated within the horizontal plane, the seismic risk estimated by the current orientation-independent PSHA method would remain the same. Although the method proposed here only includes

one of the possible causes of ground motion directionality, it can serve as a starting point to consider the dependence of horizontal orientation within PSHA.

Acknowledgements

The authors would like to thank the National Agency for Research and Development (ANID) / Doctorado Becas Chile / 2019-72200307 and the Nancy Grant Chamberlain Fellowship at Stanford University for sponsoring the doctoral studies of the first author. The authors also benefited from discussions and suggestions by professors Anne Kiremidjian and Jack Baker.

Data and Resources

The geometry and earthquake rates of the San Andreas and Hayward Faults were obtained from the Uniform California Earthquake Rupture Forecast Version 3 (UCERF3) model at https://pubs.usgs.gov/of/2013/1165 (last accessed March 2024). The ground motion records used for Figures 1 and 2 were obtained from the NGA-West2 ground motion database developed by the Pacific Earthquake Engineering Research Center (https://ngawest2.berkeley.edu/spectras/new, last accessed April 2020). Figures were made using the Python libraries Matplotlib (Hunter 2007), Cartopy (https://doi.org/10.5281/zenodo.13905945, last accessed April 2025), and PyGMT (Tian et al. 2025), a wrapper for GMT version 6 (Wessel et al. 2019).

Author note

This research was conducted while Alan Poulos was at the Department of Civil and Environmental Engineering at Stanford University. He is now at the United States Geological Survey and may be contacted at apoulos@usgs.gov.

References

Ancheta TD, Darragh RB, Stewart JP, Seyhan E, Silva WJ, Chiou BSJ, Wooddell KE, Graves RW, Kottke AR, Boore DM, Kishida T and Donahue JL (2014) NGA-West2 database. *Earthquake Spectra* 30(3): 989–1005.

Bonamassa O and Vidale JE (1991) Directional site resonances observed from aftershocks of the 18 October 1989 Loma Prieta earthquake. *Bulletin of the Seismological Society of America* 81(5): 1945–1957.

Boore DM (2010) Orientation-independent, nongeometric-mean measures of seismic intensity from two horizontal components of motion. *Bulletin of the Seismological Society of America* 100(4): 1830–1835.

Boore DM, Stewart JP, Seyhan E and Atkinson GM (2014) NGA-West2 equations for predicting PGA, PGV, and 5% damped PSA for shallow crustal earthquakes. *Earthquake Spectra* 30(3): 1057–1085.

Cornell CA (1968) Engineering seismic risk analysis. *Bulletin of the Seismological Society of America* 58(5): 1583–1606.

Esteva L (1967) Criterios para la construcción de espectros para diseño sísmico. In: *3er Simposio Panamericano de Estructuras*. Caracas, Venezuela. [in Spanish].

Esteva L (1968) *Bases para la formulación de decisiones de diseño sísmico*. PhD Thesis, Universidad Nacional Autónoma de México, Mexico City, Mexico. [in Spanish].

Field EH, Arrowsmith RJ, Biasi GP, Bird P, Dawson TE, Felzer KR, Jackson DD, Johnson KM, Jordan TH, Madden C, Michael AJ, Milner KR, Page MT, Parsons T, Powers PM, Shaw BE, Thatcher WR, Weldon RJ and Zeng

Y (2014) Uniform California earthquake rupture forecast, version 3 (UCERF3)—The time-independent model. *Bulletin of the Seismological Society of America* 104(3): 1122–1180.

Girmay N, Miranda E and Poulos A (2024a) Orientation and intensity of maximum response spectral ordinates during the December 20, 2022 Mw 6.4 Ferndale, California earthquake. *Soil Dynamics and Earthquake Engineering* 176: 108323.

Girmay N, Poulos A and Miranda E (2024b) Directionality and polarization of response spectral ordinates in the 2023 Kahramanmaras, Türkiye earthquake doublet. *Earthquake Spectra* 40(1): 486–504.

Gutenberg B and Richter CF (1944) Frequency of earthquakes in California. *Bulletin of the Seismological society of America* 34(4): 185–188.

Hong HP and Goda K (2007) Orientation-dependent ground-motion measure for seismic-hazard assessment. *Bulletin of the Seismological Society of America* 97(5): 1525–1538.

Hunter JD (2007) Matplotlib: A 2D graphics environment. *Computing in Science & Engineering* 9(03): 90–95.

Ishimoto M and Iida K (1939) Observations of earthquakes registered with the microseissmograph constructed recently. *Bulletin of the Earthquake Research Institute, University of Tokyo* 17: 443–478.

Ktenidou OJ, Chávez-García FJ, Raptakis D and Pitilakis KD (2016) Directional dependence of site effects observed near a basin edge at Aegion, Greece. *Bulletin of Earthquake Engineering* 14: 623–645.

McGuire RK (2004) Seismic hazard and risk analysis. EERI Monograph MNO-10, Earthquake Engineering Research Institute.

Petersen MD, Shumway AM, Powers PM, Field EH, Moschetti MP, Jaiswal KS, Milner KR, Rezaeian S, Frankel AD, Llenos AL, Michael AJ, Altekruse JM, Ahdi SK, Withers KB, Mueller CS, Zeng Y, Chase RE, Salditch LM, Luco N, Rukstales KS, Herrick JA, Girot DL, Aagaard BT, Bender AM, Blanpied ML, Briggs RW, Boyd OS, Clayton BS, DuRoss CB, Evans EL, Haeussler PJ, Hatem AE, Haynie KL, Hearn EH, Johnson KM, Kortum ZA, Kwong NS, Makdisi AJ, Mason HB, McNamara DE, McPhillips DF, Okubo PG, Page MT, Pollitz FF, Rubinstein JL, Shaw BE, Shen ZK, Shiro BR, Smith JA, Stephenson WJ, Thompson EM, Thompson JA, Wirth EA and Witter RC (2024) The 2023 US 50-state national seismic hazard model: Overview and implications. *Earthquake Spectra* 40(1): 5–88.

Poulos A and Miranda E (2022a) Probabilistic characterization of the directionality of horizontal earthquake response spectra. *Earthquake Engineering & Structural Dynamics* 51(9): 2077–2090.

Poulos A and Miranda E (2022b) Proposal of orientation-independent measure of intensity for earthquake-resistant design. *Earthquake Spectra* 38(1): 235–253.

Poulos A and Miranda E (2023a) Effect of style of faulting on the orientation of maximum horizontal earthquake response spectra. *Bulletin of the Seismological Society of America* 113(5): 2092–2105.

Poulos A and Miranda E (2023b) Modification of ground-motion models to estimate orientation-dependent horizontal response spectra in strike-slip earthquakes. *Bulletin of the Seismological Society of America* 113(6): 2718–2729.

Poulos A and Miranda E (2024) Directionality characteristics of horizontal response spectra from the 2022 Mw 6.9 Chihshang, Taiwan earthquake. *Earthquake Spectra* 40(3): 1683–1696.

Somerville PG, Smith NF, Graves RW and Abrahamson NA (1997) Modification of empirical strong ground motion attenuation relations to include the amplitude and duration effects of rupture directivity. *Seismological Research Letters* 68(1): 199–222.

Spudich P, Hellweg M and Lee WHK (1996) Directional topographic site response at Tarzana observed in aftershocks of the 1994 Northridge, California, earthquake: implications for mainshock motions. *Bulletin of*

the Seismological Society of America 86(1B): S193–S208.

Tian D, Uieda L, Leong WJ, Fröhlich Y, Schlitzer W, Grund M, Jones M, Toney L, Yao J, Tong JH, Magen Y, Materna K, Belem A, Newton T, Anant A, Ziebarth M, Quinn J and Wessel P (2025) *PyGMT: A Python interface for the Generic Mapping Tools (v0.15.0)*. Zenodo. DOI:10.5281/zenodo.15071586. URL https://doi.org/10.5281/zenodo.15071586.

Treiman JA, Kendrick KJ, Bryant WA, Rockwell TK and McGill SF (2002) Primary surface rupture associated with the M_w 7.1 16 October 1999 Hector Mine earthquake, San Bernardino County, California. *Bulletin of the Seismological Society of America* 92(4): 1171–1191.

Wells DL and Coppersmith KJ (1994) New empirical relationships among magnitude, rupture length, rupture width, rupture area, and surface displacement. *Bulletin of the seismological Society of America* 84(4): 974–1002.

Wessel P, Luis JF, Uieda L, Scharroo R, Wobbe F, Smith WHF and Tian D (2019) The generic mapping tools version 6. *Geochemistry, Geophysics, Geosystems* 20(11): 5556–5564.